THE ASTROPHYSICAL JOURNAL, 396:104–114, 1992 September 1

DISCOVERING PLANETARY SYSTEMS THROUGH GRAVITATIONAL MICROLENSES

ANDREW GOULD AND ABRAHAM LOEB
Institute for Advanced Study, Princeton, NJ 08540
Received 1991 December 26; accepted 1992 March 9

ABSTRACT

Planetary systems of Galactic disk stars can be detected as microlenses of stars in the Galactic bulge. Planets in a solar-like system positioned half-way to the Galactic center should leave a noticeable signature (magnification larger that 5%) on the light curve of a gravitationally lensed bulge star in $\sim 20\%$ of the microlensing events. This high probability results from a coincidence between Jupiter's orbital radius and the solar Einstein radius at this distance. Typical planetary signals last for about 1 day, a small fraction of the approximately 1 month duration of the entire microlensing event. Dedicated monitoring of microlensing candidates is suggested as a method to discover planetary systems in conjunction with forthcoming observations toward the Galactic bulge.

Subject headings: gravitational lensing — planetary systems — stars: variables: other

1. INTRODUCTION

The first discovery of planets outside the solar system was reported recently (Wolszczan & Frail 1992). These two $\sim 3\,M_\odot$ planets orbit the pulsar 1257+12 and were detected through their gravitational effects on the pulsar period. Attempts to find planets in more common environments, e.g., near main-sequence stars, have not so far been conclusive (Stevenson 1991). The traditional methods for planetary system searches involve either indirect observations (e.g., astrometry or radial velocity measurements) or direct infrared observations (see Stevenson 1991, and references therein).

In this paper we explore in detail a novel method for discovering planetary systems in the Galactic disk. The approach, first suggested by Mao & Paczyński (1991), makes use of the rare events in which the image of a bulge star is being gravitationally lensed by an intervening disk star. During such an event the brightness of the bulge star increases, peaks, and then decreases over the course of several weeks or months. The resulting light curve is smooth and completely described by three parameters, the temporal width, the maximum magnification and the time of maximum magnification. However, if planets surround the lensing star, then this well-defined light curve may be significantly altered during a time period of order days. In approximately 20% of microlensing[1] events generated by a solar-like system, the light-curve perturbations induced by the planets would be detectable. This relatively high probability obtains because of a special coincidence between the orbital radius (5.2 AU) of a Jupiter-like planet and the Einstein ring radius (4 AU) of a Solar-like star lying half-way to the Galactic center. The Einstein radius of the star is given by $(4GM\tilde{D}/c^2)^{1/2}$, where M is the mass of the star, $\tilde{D} = D_{\rm OL}\,D_{\rm LS}/D_{\rm OS}$, and $D_{\rm OL}$, $D_{\rm LS}$, and $D_{\rm OS}$ are the distances between the observer, lens, and source. A planet of mass m affects appreciably the microlensed image only if the planet and the unperturbed image are separated by of order the planet's own Einstein radius, $(4Gm\tilde{D}/c^2)^{1/2}$. The area covered by the planetary Einstein ring is smaller than that of the lensing star by (m/M), and so the probability that the image will be affected by the planet *at any given moment during the event* is likewise $\sim (m/M)$. However, as the image sweeps across the Einstein ring of the lensing star, the planetary Einstein ring sweeps through a total fractional area $\sim (m/M)^{1/2}$. This fraction is approximately 3% for Jupiter and the Sun. Naively, one may identify this fraction with the planetary detection probability if the microlensing event is monitored continuously. Nevertheless, as we show in this paper, the actual probability of detecting a Jupiter-like planet turns out to be $\sim 17\%$, much higher than this naive estimate. The difference is accounted for by the above-mentioned coincidence between the Jupiter-like orbital radius and the Sun-like Einstein radius. The probability of detecting a Saturn-like planet is $\sim 3\%$, much closer to what one would naively guess ($\sim 2\%$).

By the same argument as given above, the planet will typically affect the image magnification only for a fraction of $(m/M)^{1/2}$ of the duration of the entire microlensing event. With the typical stellar velocities (~ 200 km s^{-1}), this corresponds to a day or so for a Jupiter-mass planet.

Figure 1 presents the effect of a planet on the otherwise smooth light curve of a lensed bulge star. The diagonal box in Figure 1*a* illustrates the elongated region in which the planet has a significant influence on the lensed image. As the source moves linearly across the Einstein ring of the disk star, it intersects this box for about a day. The sharp distortion that the smooth light curve suffers during this period signals the existence of the planet.

The probability that a given bulge star will be lensed by a star in the disk is $\lesssim 10^{-6}$. Only a few per million bulge stars per year are expected to be microlensed (Paczyński 1991; Griest et al. 1991). The above method must therefore be combined with a massive search for lensing events toward the Galactic bulge. Such searches are about to be undertaken by the Macho Collaboration (Alcock et al 1992) and a Warsaw-Carnegie collaboration (Paczyński et al. 1992), having been motivated by other goals, including detection of the halo dark matter, detection of the disk dark matter, and measurement of the faint end of the present mass function of the disk (Paczyński 1991; Griest et al. 1991).

In the context of these searches Mao & Paczyński (1991) recently considered the effects of binaries and planetary

[1]The term microlensing originates from the fact that the undetectable separation between the two images is of order a micro-arcsec for a solar mass positioned at cosmological distances. However, for Galactic stars the separation is of order milli-arcsec.

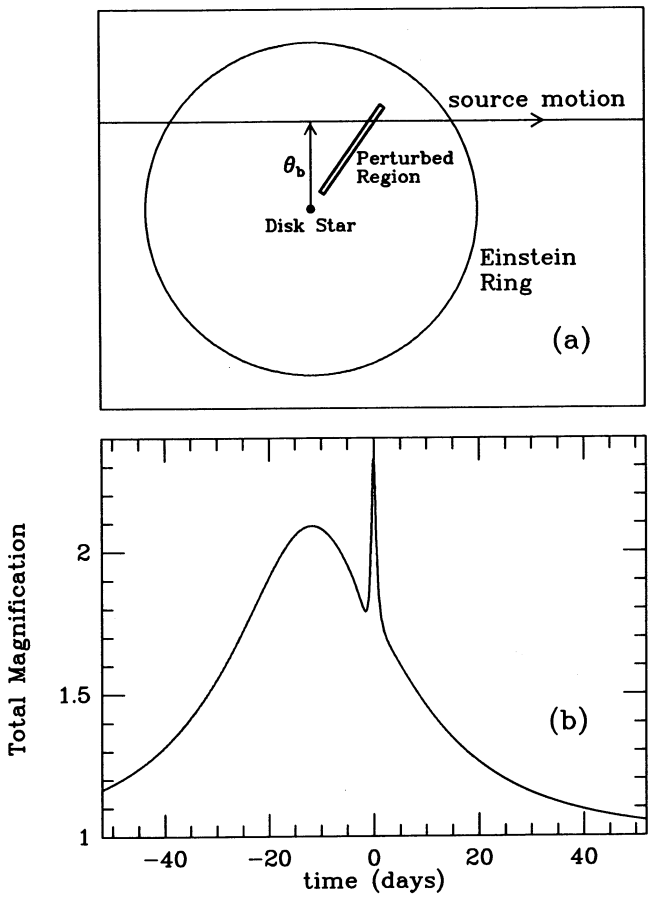

FIG. 1.—Geometry of a star-plus-planet lensing event (*a*) and resulting light curve (*b*). A bulge source star moves through the Einstein ring of a disk star with an impact parameter $\theta_b = 0.53\theta_*$, where θ_* is an Einstein ring radius. The masses of the star and planet are 1 $M_\odot$ and 10^{-3} $M_\odot$, respectively. They lie halfway to the Galactic center at 4 kpc, and their projected separation is 5.2 AU. Over most of the trajectory, the light curve is virtually unaffected by the presence of the planet. The diagonal box represents schematically the region where the light curve is affected by at least 5%. Significant deviation lasts for about 1 day.

systems on the microlensing observations toward the Galactic bulge. They analyzed briefly the effects of planets on a microlensing light curve and concluded that the detection probability is of order 3% to 10%, for a Jupiter-mass planet. In this work we extend Mao & Paczyński's analysis and explore in detail the feasibility of a dedicated search for planets using microlenses.

In § 2, we use Fermat's principle to analyze the magnification effects of a planet on a microlensed image. In § 3, we calculate the probability for detecting a planet given that the parent star passes within one Einstein radius of the source. We then apply this result to a solar-like system lying at a random position and orientation between the Earth and the Galactic bulge. We use a standard solar system for the numerical examples since it is the only system for which accurate data about the relative positions and masses of different planets exist.[2] In § 4, we examine sample light curves and estimate the distribution of temporal widths for the planet-induced perturbations to the light curve. In § 5, we outline the necessary observational effort for a dedicated microlensing search for planets. Finally, § 6 summarizes our conclusions.

[2] The source size (typically $\sim 10^{11}$ cm for a bulge giant star) can be ignored for Jupiter-like planets but must be taken into consideration for planets lighter than the Earth for which the Einstein radius is comparable to the source size. Since the lighter planets contribute a negligible probability in our examples, we treat the sources as pointlike.

2. PLANETARY PERTURBATION TO A STELLAR LENS

The images of a lensed source are positioned at the stationary points of the time delay surface induced by the lens (Fermat's principle). For a single point lens of mass M, the time delay in units of $4GM/c^3$ is given by (e.g., Blandford & Kochanek 1987)

$$\tau = \tfrac{1}{2}(\boldsymbol{x}_i - \boldsymbol{x}_s)^2 - \ln(x_i)\,, \tag{2.1}$$

where $\boldsymbol{\theta}_s = \theta_* \boldsymbol{x}_s$ and $\boldsymbol{\theta}_i = \theta_* \boldsymbol{x}_i$ are the angular positions of the source and the image relative to the lens, θ_* is the Einstein ring radius,

$$\theta_*^2 \equiv \frac{4GM}{Dc^2}\,, \quad D \equiv \frac{D_{\rm OL} D_{\rm OS}}{D_{\rm LS}}\,, \tag{2.2}$$

and $D_{\rm OL}$, $D_{\rm LS}$, and $D_{\rm OS}$ are the relative distances between the observer (O), lens (L), and source (S). The first term in equation (2.1) is the geometrical time delay while the second term arises from the gravitational redshift in the lens potential.

By the requirement that τ be stationary,

$$\partial_{\boldsymbol{x}_i}\tau = \boldsymbol{x}_i - \boldsymbol{x}_s - \frac{\boldsymbol{x}_i}{x_i^2} = 0\,, \tag{2.3}$$

there are two images located at $\theta_{i,\pm} = x_{i,\pm}\,\theta_*$,

$$x_{i,\pm} = \frac{x_s \pm (x_s^2 + 4)^{1/2}}{2}\,, \tag{2.4}$$

one inside and one outside the Einstein ring. The outer image is always brighter by a factor $x_{i,+}^4$. The combined light from the two images results in a magnification, A, of the source brightness. Since surface brightness is conserved (Liouville's theorem), the total magnification is the Jacobian of the area transformation between the image and the source coordinates, i.e.,

$$A_\pm = \left|\frac{\partial\boldsymbol{\theta}_s}{\partial\boldsymbol{\theta}_{i,\pm}}\right|^{-1} = \left|\frac{\partial^2\tau}{\partial\boldsymbol{x}_{i,\pm}^2}\right|^{-1}. \tag{2.5}$$

Thus, if a star in the Galactic bulge is lensed by an isolated foreground star in the Galactic disk, the former will be amplified by a factor

$$A(x_s) = A_+ + A_- = \frac{1}{1 - x_{i,-}^4} + \frac{1}{x_{i,+}^4 - 1} = \frac{x_s^2 + 2}{x_s(x_s^2 + 4)^{1/2}}\,. \tag{2.6}$$

Now suppose that the lensing star is not isolated, but has a single planet of mass m,

$$m = \epsilon M, \quad \epsilon \ll 1\,, \tag{2.7}$$

positioned at $\boldsymbol{\theta}_p = \boldsymbol{x}_p\theta_*$ relative to it. The magnification then differs from the value given by equation (2.6) and becomes

$$A(x_s, x_p) \equiv (1 + \delta)A(x_s)\,. \tag{2.8}$$

Equation (2.8) serves to define δ, the magnification excess. If the planet lies far from the light path (i.e., the unperturbed image position) of either of the two images, it will hardly perturb the isolated-star lensing, and $|\delta|$ will be small. On the other hand, if the planet gets near one of the image positions, it may perturb the light curve significantly, thereby allowing the planet to be "observed."

To examine the effect of the planet quantitatively, we add the planetary perturbation to the time-delay surface given by equation (2.1):

$$\tau = \tfrac{1}{2}(\boldsymbol{x}_i - \boldsymbol{x}_s)^2 - \ln|\boldsymbol{x}_i| - \epsilon \ln|\boldsymbol{x}_i - \boldsymbol{x}_p| . \tag{2.9}$$

The second and third terms arise from the potentials of the lensing star and planet, respectively. By Fermat's principle, the images are located at the solutions of

$$0 = \partial_{\boldsymbol{x}_i}\tau = \boldsymbol{x}_i - \boldsymbol{x}_s = \frac{\boldsymbol{x}_i}{x_i^2} - \epsilon \frac{\boldsymbol{x}_i - \boldsymbol{x}_p}{(\boldsymbol{x}_i - \boldsymbol{x}_p)^2} . \tag{2.10}$$

If ϵ were set to zero (i.e., no planet) we would recover the equations for the isolated star, and in particular the images would lie at their unperturbed positions. Since $\epsilon \ll 1$, we may assume that at most one image is significantly affected and that the perturbed images lie near the unperturbed image, $\boldsymbol{x}_{i0}$. It is therefore appropriate to expand equation (2.9) in a Taylor series about the unperturbed image. Since the first derivatives of τ vanish at the image position, we keep terms to second order. Using the definitions

$$(\xi_i, \eta_i) \equiv \boldsymbol{x}_i - \boldsymbol{x}_{i0} , \quad (\xi_p, \eta_p) \equiv \boldsymbol{x}_p - \boldsymbol{x}_{i0} , \tag{2.11}$$

and substituting into equation (2.9), we find

$$\tau \approx \frac{1}{2}[(1+\gamma)\xi_i^2 + (1-\gamma)\eta_i^2] - \frac{\epsilon}{2}\ln[(\xi_i - \xi_p)^2 + (\eta_i - \eta_p)^2] , \tag{2.12}$$

where

$$\gamma \equiv \frac{1}{x_{i0}^2} \tag{2.13}$$

is determined by the unperturbed image position. Equation (2.12) assumes that the sheer due to the lensing star changes little over the region of interest and takes the lens-source direction as the ξ-axis.

We find the image positions by first setting the gradient of equation (2.12) to zero, which gives

$$(1+\gamma)\xi_i = \epsilon \frac{\xi_i - \xi_p}{(\xi_i - \xi_p)^2 + (\eta_i - \eta_p)^2} ;$$
$$(1-\gamma)\eta_i = \epsilon \frac{\eta_i - \eta_p}{(\xi_i - \xi_p)^2 + (\eta_i - \eta_p)^2} . \tag{2.14}$$

The ratio of these equations yields η_i as a function of ξ_i,

$$\eta_i = \frac{(1+\gamma)\eta_p \xi_i}{2\gamma\xi_i + (1-\gamma)\xi_p} . \tag{2.15}$$

Substituting equation (2.15) into the first of equations (2.14) then results in a quartic equation for ξ_i,

$$\xi_i^4 + \frac{(1-2\gamma)\xi_p}{\gamma}\xi_i^3 + \left[\frac{(1-\gamma)^2(\xi_p^2+\eta_p^2)}{4\gamma^2} - \frac{(1-\gamma)\xi_p^2}{\gamma} - \frac{\epsilon}{1+\gamma}\right]\xi_i^2 - \left[\frac{(1-\gamma)^2(\xi_p^2+\eta_p^2)\xi_p}{4\gamma^2} + \frac{\epsilon(1-\gamma)\xi_p}{\gamma(1+\gamma)}\right]\xi_i - \frac{\epsilon(1-\gamma)^2\xi_p^2}{4\gamma^2(1+\gamma)} = 0 . \tag{2.16}$$

Equation (2.16) can be solved algebraically (Abramowitz & Stegun 1972). There are always either two or four roots. These may be substituted into the magnification formula obtained by applying equation (2.5) to equation (2.12),

$$A = \left| 1 - \left\{ \gamma + \epsilon \frac{(\xi_i - \xi_p)^2 - (\eta_i - \eta_p)^2}{[(\xi_i - \xi_p)^2 + (\eta_i - \eta_p)^2]^2} \right\}^2 - 4\epsilon^2 \frac{(\xi_i - \xi_p)^2(\eta_i - \eta_p)^2}{[(\xi_i - \xi_p)^2 + (\eta_i - \eta_p)^2]^4} \right|^{-1} . \tag{2.17}$$

The magnification contour structure in the lens plane can be obtained directly from equations (2.16) and (2.17) for given values of ϵ and γ. Figures 2*a–d* present the excess magnification associated with the planet {i.e., $\delta \equiv [A(\xi_p, \eta_p)/A(x_s) - 1]$} as a function of (ξ_p, η_p) for $\gamma = 0.6$, 0.9, 1.2, and 1.6. The contours reflect the way that the magnification would change if the planet were moved around relative to a fixed source-lens orientation. This contour structure will be useful in the following section for evaluation of the planet detection probabilities. In order to obtain the light curves of the lensed bulged star one must transform the magnification contours from the planet coordinates in the lens plane, $\boldsymbol{x}_p$, to the source coordinates, $\boldsymbol{x}_s$, in the source plane. The magnification contours will then reflect the way that the magnification changes as the source moves around while the planet-star orientation remains fixed. This transformation can be obtained from equation (2.11), and the fact that the source, the lensing star, and the unperturbed image are collinear, namely (see eq. [2.4])

$$\boldsymbol{x}_{i0} = \frac{x_{i0}}{x_s}\boldsymbol{x}_s . \tag{2.18}$$

Figures 3*a–3d* presents the excess magnification contours in the source plane for $\boldsymbol{x}_p = (0.5, 0)$, (0.7, 0), (1.3, 0), and (2.2, 0). The value $\boldsymbol{x}_p = (1.3, 0)$ is characteristic for a Jupiter-like planet. The line of infinite magnification (the critical line) is diamond-shaped. When the planet is near the stellar Einstein radius, $x_p \sim 1$, the weak-magnification contours are stretched along the planet-star axis.[3] In this case, the region of source plane which is affected by at least 5% forms roughly the shape of an elongated box. The width of this box is typically $\sim\epsilon^{1/2}$, although it is slightly wider or narrower in some places (see, e.g., Figs. 3*b* and 3*c*). We will make use of this boxlike structure when we analyze the event durations in § 4.

3. PLANETARY DETECTION PROBABILITIES

We now calculate the probability that a planetary system can be detected, given that the source passes within the Einstein ring of its central star. This can be done by first calculating the probability distribution of the planet's position in the lens plane, and then finding the region of the lens plane where the planet can be detected.

3.1. *Planet Distribution on the Einstein Ring*

Suppose that a star of mass M with a single planet of mass, $m = \epsilon M$, and circular orbital radius, a, lies at a distance $D_{\rm OL}$

[3] We have compared the magnification contours shown in Figure 3*c*, derived using the approximate time-delay surface, equation (2.12), with an exact numerical calculation generously provided to us by J. Wambsganss. We find very good agreement. The only noticeable difference is that the leftward arching of the caustics in Figure 3*c* is not present in the exact calculation. This difference has no significant effect on the results reported in this paper.

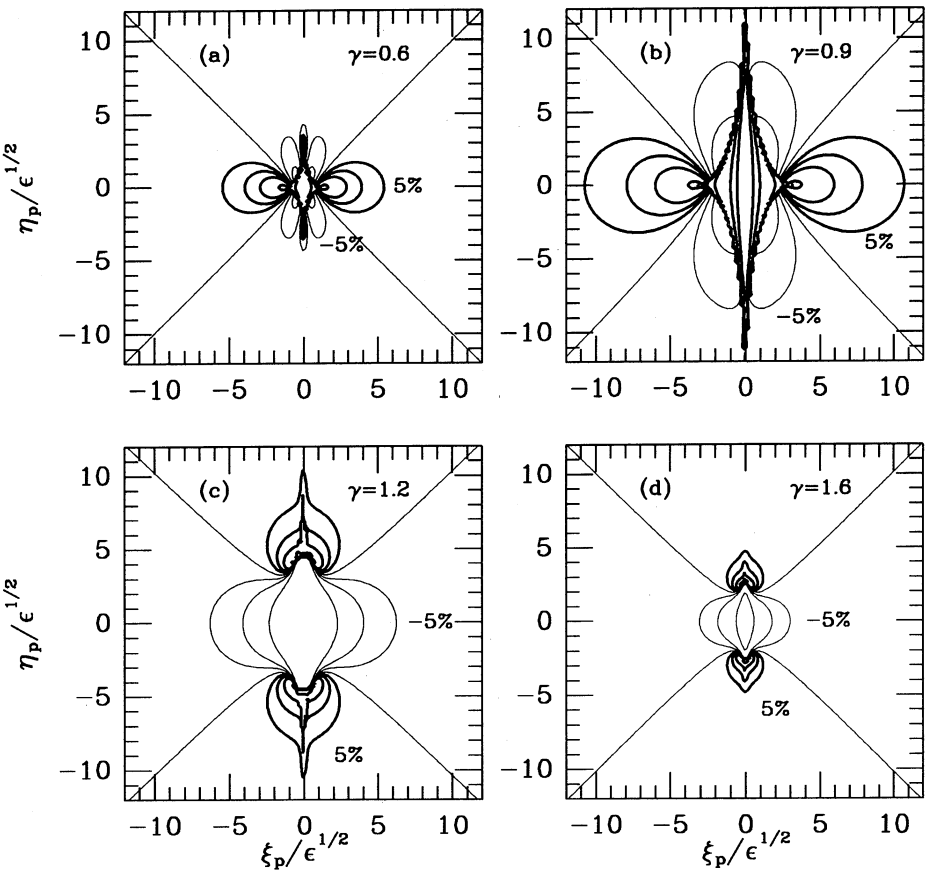

FIG. 2.—Planetary magnification in the lens plane as a function of the planet position x_p for fixed lens-source orientations of $\gamma = 0.6$ (*a*), 0.9 (*b*), 1.2 (*c*), and 1.6 (*d*). The contour set represents excess planetary magnifications of $\delta \equiv (A[x_s, x_p]/A[x_s] - 1) = -20\%, -10\%, -5\%, 0, 5\%, 10\%, 20\%, 100\%$, and 300%. Positive contours are bold. The $\pm 5\%$ contours are marked. In the limit $\gamma \to 0$ the diamond-shaped critical line shrinks to a point, while the surrounding contours become circular as is appropriate for an isolated point mass. In the limit $\gamma \to \infty$ the closed positive-contour structure shrinks into two separated points. The $\pm 5\%$ contours are used to bracket the detection probabilities in the following section. Results are valid for arbitrary mass ratio, $\epsilon \equiv (m/M) \ll 1$.

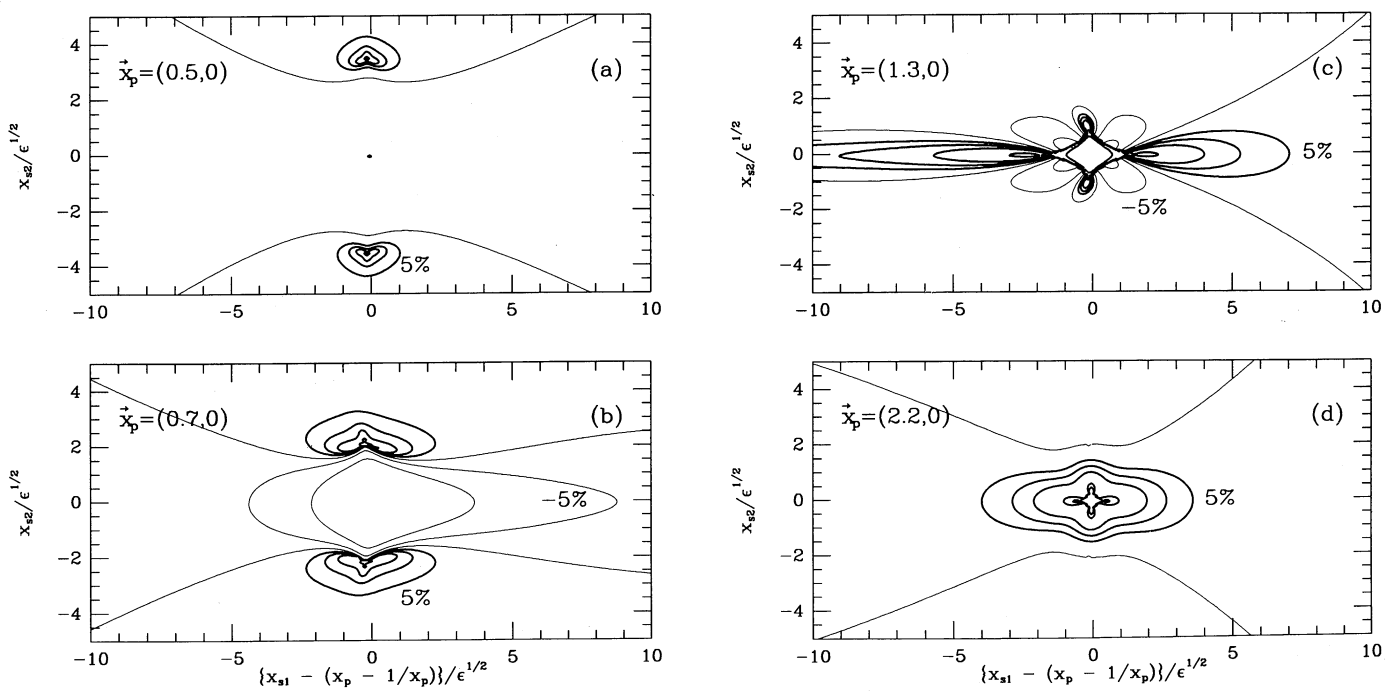

FIG. 3.—Magnification contours in the source plane x_s for a planet located at $x_p = (0.5, 0)$ (*a*); (0.7, 0) (*b*); (1.3, 0) (*c*); and (2.2, 0) (*d*). The set of contours represent the excess planetary magnifications of $\delta = -20\%, -10\%, -5\%, 0, 5\%, 10\%, 20\%, 100\%$, and 300%. Positive contours are bold. The $\pm 5\%$ contours are marked. Results are valid for arbitrary mass ratio, $\epsilon \equiv (m/M) \ll 1$.

from the Earth. Since the typical planetary speed is ~ 10 km s^{-1}, while the typical speed of the source relative to the planetary system is ~ 200 km s^{-1}, the planet's orbital position may be considered as fixed during the lensing event. We consider an ensemble of such systems having random inclinations, random orbital phases, and a density distribution, $\nu(z)$, along the line of sight between the Earth and the Galactic bulge, where

$$z \equiv \frac{D_{\rm OL}}{D_{\rm OS}} . \tag{3.1}$$

We first determine the distribution of r, the *physical* projected separation of the planet from its central star. Putting the planetary orbit at a random inclination and phase is equivalent to putting the planet at a random position on a sphere of radius a. Therefore, the probability distribution, $p(r)$, is given by

$$p(r) = \frac{r}{a^2}\left(1 - \frac{r^2}{a^2}\right)^{-1/2} \qquad (0 \le r \le a) , \tag{3.2}$$

and the cumulative distribution, $F(r)$, by

$$F(r) \equiv \int_r^a dr\, p(r) = \left(1 - \frac{r^2}{a^2}\right)^{1/2} . \tag{3.3}$$

Next we find the cumulative distribution $F(x_p \,|\, z)$, where

$$x_p \equiv \frac{r}{D_{\rm OL}\,\theta_*(z)} \tag{3.4}$$

is the projected position of the planet at fractional distance z in units of the Einstein radius. Equations (2.2), (3.1), (3.3), and (3.4) imply

$$F(x_p \,|\, z) = \left[1 - 4z(1-z)\,\frac{x_p^2}{x_*^2}\right]^{1/2} , \tag{3.5}$$

where

$$x_* \equiv \frac{ac}{(GMD_{\rm OS})^{1/2}} \approx 0.25\left(\frac{a}{\rm AU}\right)\left(\frac{M}{M_\odot}\right)^{-1/2}\left(\frac{D_{\rm OS}}{8\ \rm kpc}\right)^{-1/2} . \tag{3.6}$$

The full cumulative distribution (weighted by probability that the source passes inside the Einstein ring) then equals

$$F(x_p) = \frac{\int_0^1 dz\theta_*(z)D_{\rm OL}(z)\nu(z)F(x_p \,|\, z)}{\int_0^1 dz\theta_*(z)D_{\rm OL}(z)\nu(z)} . \tag{3.7}$$

Equation (3.7) can be simplified somewhat by noting that both $(\theta_*\, D_{\rm OL})$ and $F(x_p \,|\, z)$ are invariant under $z \to (1 - z)$. Hence, we can replace $\nu(z) \to [\nu(z) + \nu(1 - z)]$. Using this substitution and changing variables to $q \equiv (1 - 2z)$, we find

$$F(x_p) = \int_0^1 dq(1-q^2)^{1/2}\left[1 - (1-q^2)\,\frac{x_p^2}{x_*^2}\right]^{1/2}\tilde{\nu}(q) \Bigg/ \int_0^1 dq(1-q^2)^{1/2}\tilde{\nu}(q) , \tag{3.8}$$

where

$$\tilde{\nu}(q) \equiv \nu[(1+q)/2] + \nu[(1-q)/2] . \tag{3.9}$$

We now adopt the following simple model for $\nu(z)$. We assume that the disk has an exponential scale length, $h \sim 4$ kpc, and a uniform exponential scale height $d \sim 300$ pc. If the line of sight is at small Galactic latitude, b radians, then

$$\nu(z) \propto \exp\,(zD_{\rm OL}/h - z\,|\,b\,|D_{\rm OL}/d).$$

Hence,

$$\tilde{\nu}(q) = C\,\cosh\left[q\,\frac{D_{\rm OS}}{2}\left(\frac{1}{h} - \frac{|\,b\,|}{d}\right)\right] , \tag{3.10}$$

where C is a constant. For $b \sim 4°$, $\tilde{\nu}(q)$ is approximately independent of q. In our illustrative examples, we will therefore adopt $\tilde{\nu} = $ const, so that

$$F(x_p) = \frac{4}{\pi}\int_0^1 dq(1-q^2)^{1/2}\left[1 - (1-q^2)\,\frac{x_p^2}{x_*^2}\right]^{1/2} . \tag{3.11}$$

The probability distribution, $p(x_p) \equiv -F'(x_p)$ is strongly peaked near $x_p = x_*$, as is clear from Figure 4 below.

3.2. *Detection Probabilities*

Consider the magnification structure in the source plane shown in Figures 3*a–d* and imagine a source moving at a constant velocity, at an arbitrary angle, and with an arbitrary impact parameter. On almost all such orbits, the planet significantly affects the magnification for at most a fraction of the time that the source spends within the star's Einstein ring. Except during this small fraction of the orbit, the observed light curve will look almost exactly like the light curve of an isolated star. Hence, the signature of a planet is a very short-lived deviation from an otherwise standard microlensing light curve (see Fig. 1.). We assume that if this deviation from a standard light curve reaches some minimum level, $\delta_{\rm min}$, then the planet can be detected. Using this assumption, we now estimate the probability that the planet will be detected given that the source passes within the Einstein ring of the lensing star.

In principle, one could find the region of the lens plane where the planet would have a significant effect as follows. First, choose an impact parameter, θ_b, for the source trajectory. Second, for each source position, find the unperturbed image position and then, using this position and the approximate time-delay surface (e.q. [2.12]), find the domain of planetary positions where the magnification deviation is at least $\delta_{\rm min}$, say 5%. Examples of such regions are shown in Figure 2. Third, find the union of all such domains as the source moves on its trajectory. Fourth, find the probability that the planet actually lies in this domain from equation (3.11). Finally, repeat the procedure for all impact parameters, $0 < \theta_b < \theta_*$.

We carry out this procedure below, but with one modification. Instead of finding the domain swept out by the *entire* $\pm\delta_{\rm min}$ contours in Figure 2, we find the domain swept by the *extreme* radial (i.e., x-axis) extent of these contours. This approximation causes us to underestimate the affected region of the lens plane and hence the probability of detection. However, we show below that the induced error is negligible. Moreover, this approximation greatly simplifies the calculation because the radial extent of the contours can be calculated almost analytically, not only for the approximate time-delay surface (e.q. [2.12]) but even for the exact time-delay surface (e.q. [2.9]). When the source, star, and planet are aligned, equation (2.10) becomes a simple cubic,

$$x_i^3 - (x_s + x_p)x_i^2 + (x_p x_s - 1 - \epsilon)x_i + x_p = 0 , \tag{3.12}$$

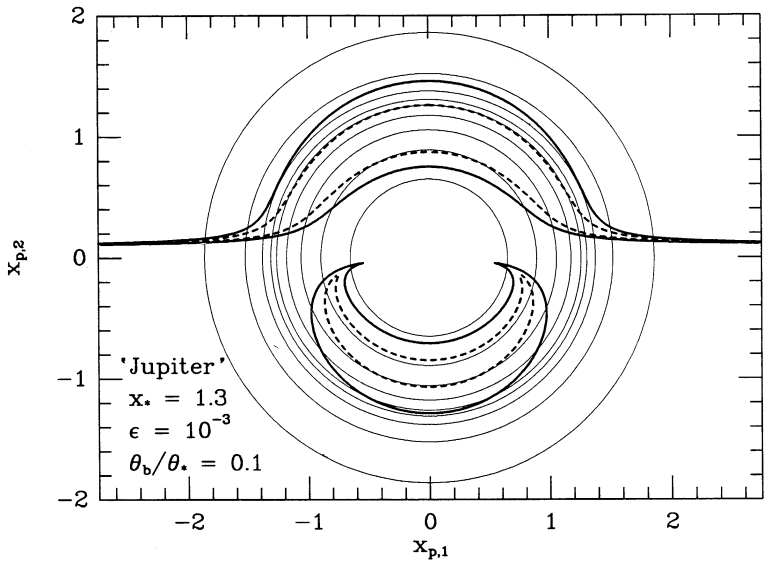

FIG. 4.—Probability distribution of a Jupiter-like planet ($\epsilon = 10^{-3}, x_* = 1.3$) on the lens plane (*circles*) and contours of constant perturbation $\delta_{min} = \pm 5\%$ (*bold solid*) and $\pm 20\%$ (*bold dashed*). Angular distances are in units of the Einstein ring, θ_*. Impact parameter is $\theta_b = 0.1\theta_*$. The area between successive concentric circles contains 10% of the planet's probability. The bold contours in the upper part of the figure are positive perturbations and arise when the planet is close to the brighter unperturbed image. Those in the lower part of the figure are negative and arise when the planet is close to the fainter unperturbed image.

which can be solved algebraically (Abramowitz & Stegun 1972). The magnification for each image is then [eq. (2.5)]

$$A = |1 - [x_i^{-2} + \epsilon(x_i - x_p)^{-2}]^2|^{-1} . \quad (3.13)$$

By taking the sum of the magnifications of the three images and comparing it with the unperturbed magnification, (e.q. [2.6]), we obtain the perturbation, δ.

Figure 4 shows the region of the lens plane enclosed by the $\delta_{min} = 5\%$ (*bold solid*) and 20% (*bold dashed*) for the case of a Jupiter-like planet in orbit about a Sun-like star. That is, we take $\epsilon = 10^{-3}$, $a = 5.2$ AU, and $x_* = 1.3$. The source is assumed to have an impact parameter $\theta_b = 0.1\theta_*$ relative to the lensing star. The circles represent cumulative probability contours, 10%, 20%, . . ., 90%, for the position of the planet. The contours in the upper part of the diagram are for an increase, $\delta = +\delta_{min}$, relative to the unperturbed signal. They arise when the planet lies near the brighter unperturbed image. The lower contours are for a decrease, $\delta = -\delta_{min}$. They arise when the planet is near the fainter unperturbed image. If the planet lies anywhere within the contours, it will perturb the image by at least δ_{min} sometime during the event. Figures 5 and 6 are similar to Figure 4, except that the impact parameters are $\theta_b = 0.4\theta_*$ and $\theta_b = 1.0\theta_*$ respectively, and only the $\delta_{min} = 5\%$ contours are shown.

Figure 7 shows a Saturn-like planet ($\epsilon = 3 \times 10^{-4}, x_* = 2.3$) with $\theta_b = 0.1\theta_*$. Comparing this with the analogous Figure 4, for a Jupiter-like planet, two important differences are apparent. First, the bold contours enclose a smaller area because

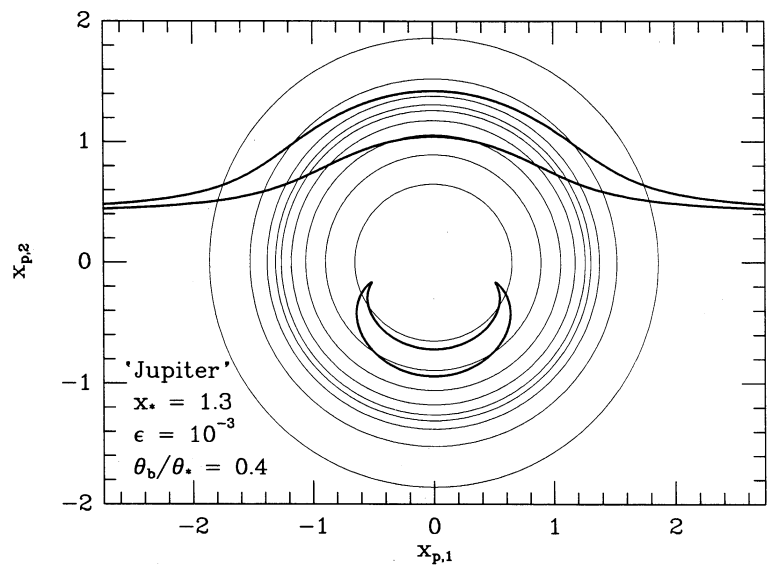

FIG. 5.—Probability distribution of a Jupiter-like planet on the lens plane (*circles*) and contours of constant perturbation $\delta_{min} = \pm 5\%$. Similar to Fig. 4, except that the impact parameter is $\theta_b = 0.4\theta_*$ and only one contour is shown.

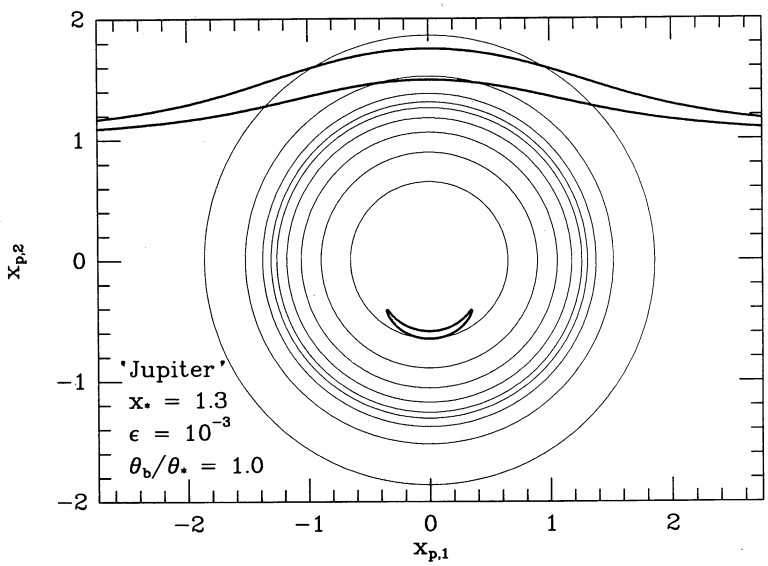

FIG. 6.—Probability distribution of a Jupiter like planet on the lens plane (*circles*) and contours of constant perturbation $\delta_{min} = \pm 5\%$. Similar to Fig. 4, except that impact parameter is $\theta_b = 1.0\theta_*$ and only one contour is shown.

Saturn is less massive than Jupiter. The width of the contours scales as $\sim\epsilon^{1/2}$. Second, and far more dramatically, the contours are much less favorably placed relative to the probability distribution of the planet. That is, the contours are concentrated near the Einstein ring, while the Saturn-like planet's probability is concentrated at more than two Einstein radii.

In Figure 8, we show the probability that a planet can be detected as a function of its orbital-radius parameter, x_*, and for various values of δ_{min}. In plotting the figure, we have assumed that $\epsilon = 10^{-3}$. For other values of ϵ, the probability scales as $\sim\epsilon^{1/2}$. Note that for each δ_{min}, there are two strong peaks, one at $x_* \sim 0.8$ where the highest planetary probability crosses the inner contours, and one at $x_* \sim 1.3$, where the highest planetary probability crosses the outer contours (see Figs. 4–7). The contributions from the inner and outer contours are shown separately for the case $\delta_{min} = 20\%$.

From Figure 8, we find that if a solar-like planetary system lay at a random position along the line of sight to the bulge, and if a bulge source came within one Einstein radius of the central star of this system, then the system could be detected $\sim 20\%$ of the time (assuming $\delta_{min} = 5\%$). By far the largest contributor would be Jupiter, partly because it is the largest planet, but primarily because its dimensionless radius, $x_* = 1.3$, lies right at the peak of the curve in Figure 8. Jupiter would contribute $\sim 17\%$, Saturn $\sim 3\%$, and all the other planets $\ll 1\%$.

Is Jupiter's extremely favorable dimensionless radius, $x_* = 1.3$, likely to be repeated in other planetary systems? A plausible if speculative argument can be made that it will be. Jupiter formed near a_{min}, the innermost radius of the proto-planetary accretion disk at which water ice condensed. Stevenson & Lunine (1988) have argued that the formation of the most

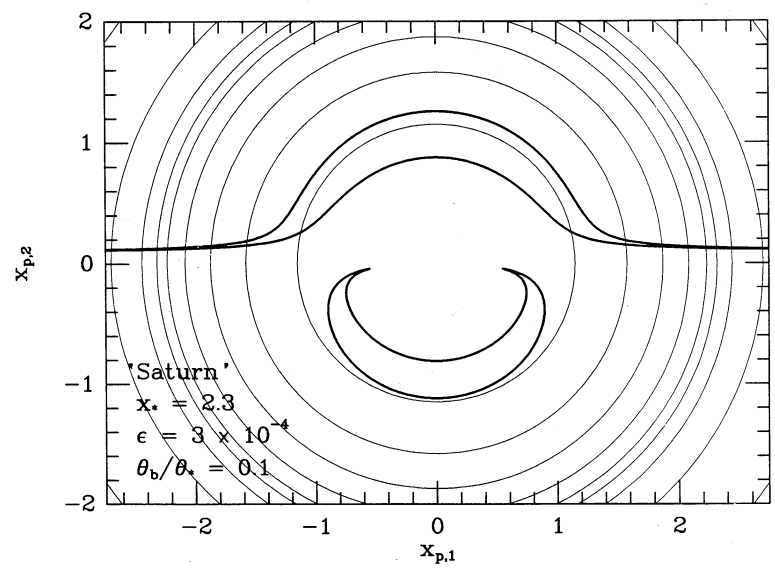

Fig. 7.—Probability distribution of a Saturn-like planet on the lens plane (*circles*) and contours of constant perturbation $\delta_{min} = \pm 5\%$. Similar to Fig. 4, except that $\epsilon = 3 \times 10^{-4}$, $x_* = 2.3$, and only one contour is shown.

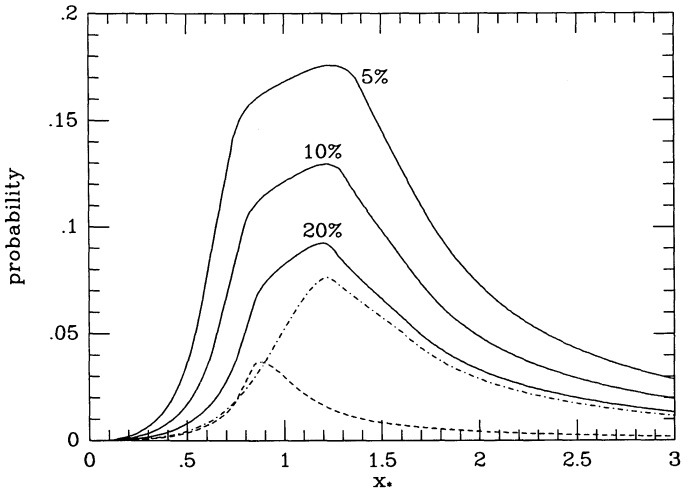

FIG. 8.—Probability for detecting a planet of orbital-radius parameter, x_* (see eq. [3.6]) given that the source passes within one Einstein radius of the central star. Total probabilities (*solid curves*) are shown for $\epsilon = 10^{-3}$, assuming that the minimum detectable perturbations are $\delta_{\min} = 5\%$, 10%, and 20%. For the last case, the probabilities for perturbation of the inner (*dashes*) and the outer (*dot-dashes*) images are shown separately.

massive planet is triggered by a "cold finger" of ice at just this point. The position of this cold finger is expected to scale as $a_{\min} \propto M^{\alpha}$, where M is the mass of the star and α is a model-dependent parameter. We are thus led to estimate (see eq. [3.6])

$$x_* \sim 1.3\left(\frac{M}{M_\odot}\right)^{\alpha - 1/2}, \tag{3.14}$$

for the dimensionless orbital radius of the most massive planet. Plausible values of α lie in the range $\frac{1}{3} \lesssim \alpha \lesssim \frac{7}{9}$ (D. Stevenson, private communication). For this range of α and for $0.2\ M_\odot \lesssim M \lesssim 2\ M_\odot$, the dimensionless radius is bounded by $0.8 \lesssim x_* \lesssim 1.7$. As shown in Figure 8, the probability of detection is substantial for these values.

We now pause to estimate the error induced by using the region swept by radial extent of the contours, instead of the region swept by the full contours (see Figs. 2*a–d*). First consider Figure 4. The width of the upper enclosed region of the 5% (*solid*) region goes to zero very quickly at the sides of the diagram. However, it is clear from Figure 3*d*, that for small γ (and hence large $x_{i,0}$) the planet can lie anywhere within a fairly large circle of the unperturbed image and still affect the image. In fact, in the limit where the planet is well outside the star's Einstein radius, the planet may be treated as an isolated lens. Then the entire region within two planet Einstein radii (i.e., $2\epsilon^{1/2}\theta_*$) will be affected by $\gtrsim 6\%$. Thus, the bold lines in Figure 4 should never get closer than about 0.12. It is clear at least in this case, however, that the correction is extremely small: first, because this width is small compared to the width of the region which dominates the diagram and second, because the planet has a very small probability of lying in this ignored region. Nevertheless, for a planet with a larger radius (see, e.g., Fig. 7), the planetary probability will be more concentrated in the ignored region and at sufficiently large planetary radius, the ignored region will actually dominate the true probability of detection. However, it turns out that the total probability of detection in this limit is given exactly by $8\epsilon^{1/2}/3\pi x_* \sim \epsilon^{1/2}/x_*$. That is, for Saturn this extreme calculation gives 0.7% compared to the actual value of 3%. Thus, it is only for planets with still larger orbital radii (and hence negligible probability of detection) for which the ignored region becomes relatively important. One can make a similar argument regarding the ignored region near the lower contour of Figure 4.

4. LIGHT CURVES

The light curve of a moving source is obtained by slicing the magnification contours in the $\boldsymbol{x}_s$ plane (see, e.g., Fig. 3) along a straight line. For fixed lens and observer positions and a source transverse velocity, $\boldsymbol{v}_r$, the temporal units of the event are fixed by the planetary Einstein ring crossing time, $D_{\rm OL}\epsilon^{1/2}\theta_*/v_T$. The distribution of these time scales for a Jupiter-mass planet is shown (*dashes*) in Figure 9. Also shown is the distribution of planetary event time scales (*solid*). The latter is computed by assuming that the region affected by the planet is a long box of width $\sim\epsilon^{1/2}\theta_*$ (see, e.g., Figs 3*c* and 1*a*). That is, for each time scale Δt shown in the dashed curve, there is a relative probability, $\cos\phi\, d\phi$ that the source trajectory will intersect the box at angle ϕ, yielding an event of duration $\Delta t/\cos\phi$.

In Figure 10, we have reproduced the source plane structure of Figure 3*c* and drawn four source trajectories through it. Figures 10A–D show the four light curves corresponding to these linear slices. Figure 10D is the same case illustrated in Figure 1. From Figure 10, it is clear that there are essentially two broad classes of light curves: those which do not intersect the caustic structure, and those which do. Figures 10A and 10D are examples of the former class and Figures 10B and 10C are examples of the latter. For the geometry shown in Figure 10, noncaustic-crossing trajectories are about 6 times more probable than their more striking counterparts. The elongated-box geometry shown in Figure 10 is typical for planets near the stellar Einstein ring. Recall from the discussion in § 3 that it is only when the planet lies fairly near the Einstein ring that it has a substantial probability of being detected. Therefore, light curve deviations of the type shown in Figures 10A and 10D are

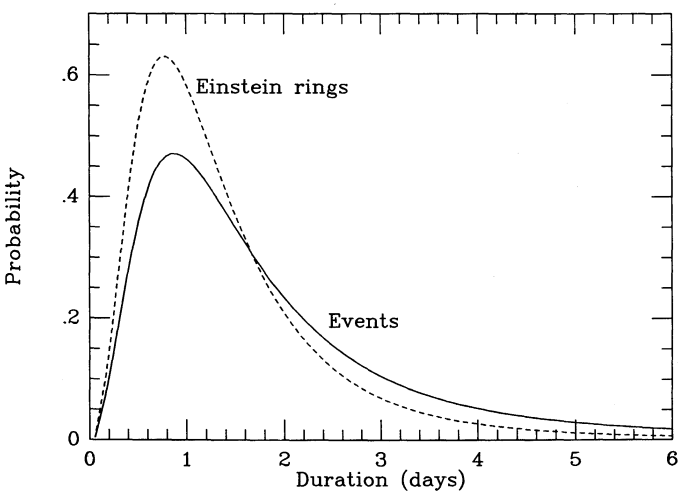

FIG. 9.—Distribution of lensing time scales for a Jupiter-mass planet ($m = 10^{-3}\ M_\odot$). The dashed curve is the distribution of planetary Einstein ring crossing times, $D_{\rm OL}\epsilon^{1/2}\theta_*/v_T$. The distribution of event times (*solid*) is computed by treating the "event zone" as a long box of width $\sim\epsilon^{1/2}\theta_*$ (see Figs. 3*c* and 1*a*). The computation assumed a uniform distribution along the line of sight to the bulge ($b \sim 4°$), a flat rotation curve for the Galactic disk, and a Gaussian velocity distribution with one-dimensional dispersion of 110 km s^{-1}.

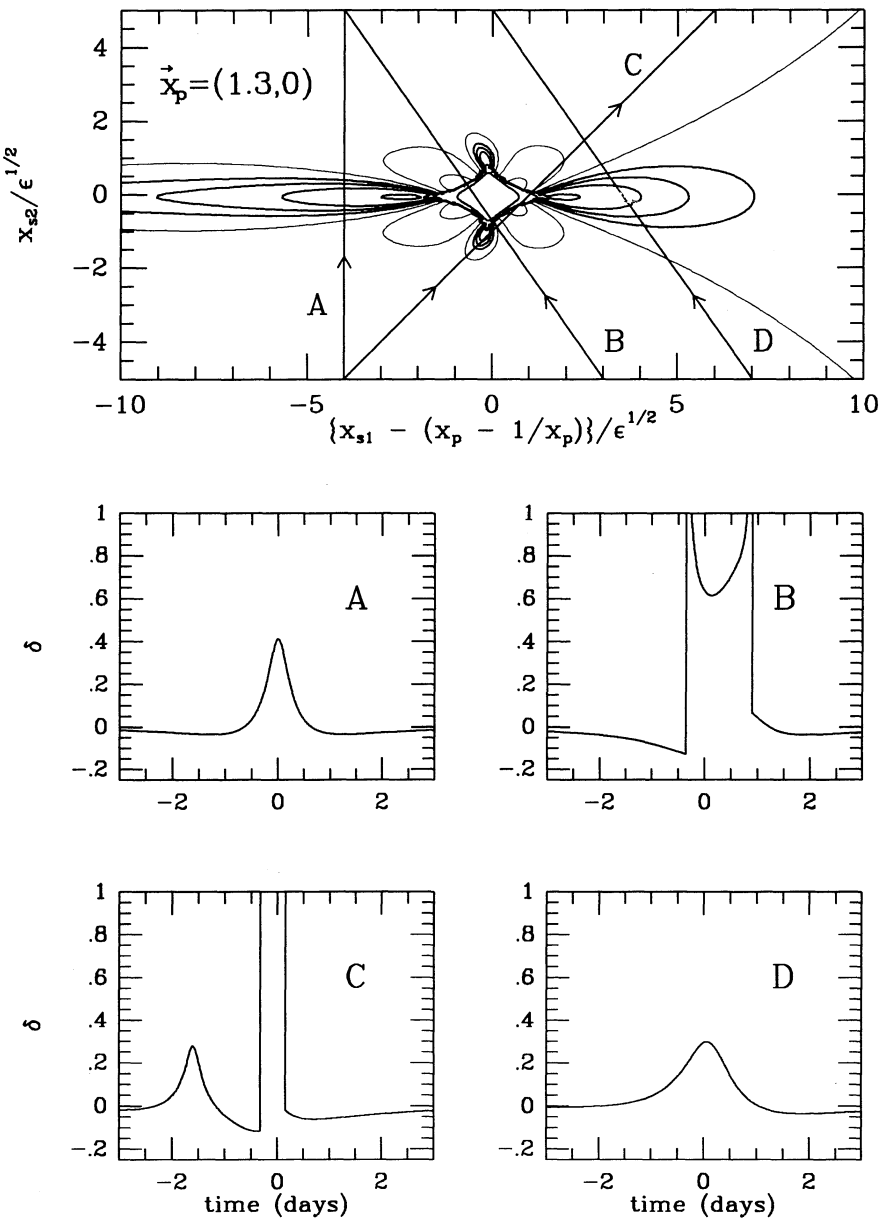

FIG. 10.—Excess light curves associated with various source trajectories through the planetary magnification structure of Fig. 3*c*. The light curves in figures A, B, C, and D correspond to the trajectories A, B, C, and D in the source plane at the top. These curves are obtained after subtraction of the original microlensing light curve. At time $t = 0$ the source passes through $x_{s2} = 0$. Trajectory D is exactly the same case illustrated in Fig. 1. The angular velocity of the source relative to the lens was taken as one planetary Einstein radius per day. The relative probability of other time scales is shown as the dashed curve in Fig. 9.

more or less typical of those likely to be seen in actual observations.

From the light curve alone, it is possible to measure the mass ratio, ϵ, but not the mass of the planet. The procedure is as follows. From the smooth part of the overall light curve (ignoring for the moment the short deviation caused by the planet), it is possible to measure the temporal width of the event and the dimensionless impact parameter, θ_b/θ_* (see, e.g., Fig. 1*b*). Then from the position of the deviation on the light curve, one may determine the value of γ as well as the orientation of the star planet vector relative to the direction of the motion of the source. These two parameters specify the contour structure (see Fig. 3) and the angle at which the source cuts the boxlike contours (see Fig. 10). The maximum magnification then gives the intercept of the source with the box axis up to an overall ambiguity. It may be possible to resolve this ambiguity from the detailed light curve since the structure of the contours is substantially different on the two sides of the planet. The duration of the deviation is given by $\alpha D_{\rm OL}\epsilon^{1/2}\theta_*/v_T$, where α is a parameter of order unity which can be calculated from the appropriate contour diagram. The measured time scale of the full event specifies $D_{\rm OL}\theta_*/v_T$. Hence, one may infer the mass ratio, ϵ. Without additional information, the individual masses of the star and planet can be estimated only statistically.

However, if the lensing star is a G dwarf or earlier, one may determine not only the planet's mass but also its projected separation. In this case, the lensing star would be $\lesssim$6.5 mag,

while the typical lensed bulge star might be ~ 2.5 mag. Since the lensing star is typically at half the bulge distance, it should be $\gtrsim 10\%$ as bright as the bulge star. Since the two stars will differ in radial velocity by ~ 100 km s^{-1}, it should be possible to resolve them spectroscopically (after the lensing event is over). From the spectral type one may determine the mass of the star, M, and hence the mass of the planet $m = \epsilon M$. Moreover, from the spectral analysis as well as the light curve, it should be possible to estimate the separate luminosities of the two stars. The apparent luminosity and spectral type of the lensing star would give D_{OL}, and hence the physical projected separation of the planet and star.

We note that the light curve due to lensing by a planetary system is easily distinguished from that due to a binary-star system. For planetary systems, the light curve deviates from a standard, single-star light curve only for a small fraction of the entire event (see Figs. 10A–D). For a binary, the light curve deviates from the standard one for a large fraction of the event (Mao & Paczyński 1991).

5. OBSERVATIONAL REQUIREMENTS

Two distinct steps are required to observe a planetary system by microlensing. First, one must single out a disk star which happens to be microlensing a bulge star. Second, one must observe this star often enough to catch the deviation in the light curve due to the planet. The first step involves the observation of millions of bulge stars on the order of once per day. The second step involves the observation of a handful of stars many times per day. In the following we give a rough outline of what is required for each of these steps.

The probability that a given bulge star is lensed by a disk star is $\sim 4 \times 10^{-7}$ (Paczyński 1991; Griest et al. 1991). A typical event lasts ~ 1 month for a solar mass lens, and scales $\propto M^{1/2}$ for other masses. The event rate is dominated by low-mass stars which have time scales of a few weeks. Thus, there are ~ 2–7×10^{-6} events per year per bulge star observed (Griest et al. 1991). The uncertainty arises from the uncertainty in the low end of the disk mass function (Scalo 1986). Figure 11 shows the expected number of events per bulge star observed for 0.1 $M_\odot$ bins. As in previous rate estimates, we have assumed a line of sight, $b \sim 4°$, where the stellar density is approximately constant. The dominant uncertainties in the figure are for $M \lesssim 0.2\, M_\odot$.

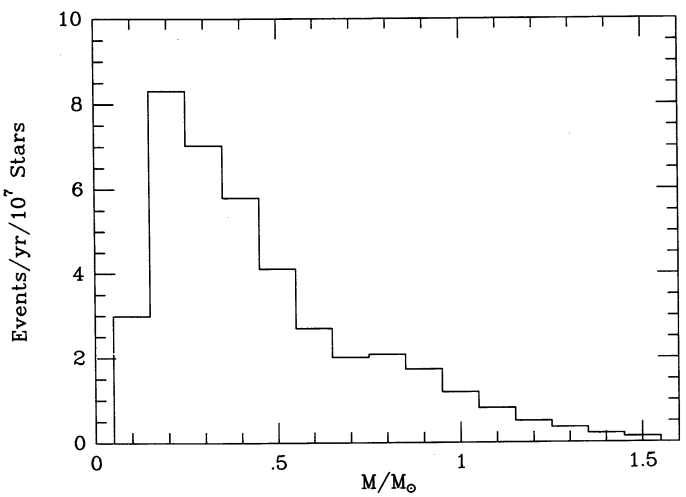

FIG. 11.—Number of expected stellar lensing events per 10^7 bulge stars observed per year. Bins are 0.1 $M_\odot$. Estimates are based on the mass function of Scalo (1986) and a stellar density which is constant along the line of sight to the bulge (i.e., $b \sim 4°$). Note that there are $\sim$eight events per yr for "solar-type" stars ($0.7 \lesssim M/M_\odot \lesssim 1.3$). Rates for stars, $M \lesssim 0.2\, M_\odot$ are uncertain.

If 10^7 bulge stars were observed, there would be $\sim$four events occurring at a given time, and $\sim$20–70 events per year. Here, an "event" means that the source and stellar lens are separated by less than one Einstein radius. Two questions arise in this context. First, are there this many stars in the Galactic bulge which can be observed? Second, can they all be imaged in a single night? Assume that about 10% of the Galactic bulge can be observed through "windows" in the obscuring dust of the Galactic disk. The crowding limit of a typical window occurs in exposures reaching stars ~ 3 mag. The total luminosity of the bulge is $\sim 2 \times 10^9\, L_\odot$ (Binney & Tremaine 1987). Hence, $\gtrsim 10^7$ stars should be observable. A more accurate estimate will be available when the Macho Collaboration begins their bulge observations in the 1992 southern winter (K. Griest, private communication). A 50 inch (1.3 m) telescope (such as the one which will actually be used by the Macho Collaboration) can reach the crowding limit in about 1 minute. Allowing another minute for readout, $\gtrsim 200$ fields per night could be observed. Thus, with a 0.5 square degree CCD Array, the entire bulge could easily be covered in a night. Since the windows are present in only parts of the bulge, it may even be possible to cover the bulge twice per night. The data produced by such a set of observations are comparable to the expected data from the Macho Collaboration's observations of the Large Magellanic Cloud (LMC).

As mentioned above, the Macho Collaboration will be observing the bulge as well as the LMC. However, because the LMC is the project's main priority, the bulge will be observed only for the ~ 4 months per year when the LMC is down. Because most of their computer facilities will be tied up in LMC work, the Macho Collaboration may choose to observe many fewer than 10^7 stars. Nevertheless, specifications of the Macho Collaboration project indicate that monitoring of 10^7 stars on a nearly year round basis is possible, and the project itself should reach a significant fraction of this observation rate.

The signature of a planet is a deviation from the standard light curve which lasts of order 1 day or less. Figure 9 shows the approximate distribution of time periods that the deviation will exceed $|\delta_{min}| \gtrsim 5\%$ for a Jupiter-mass planet. For planets of other masses m, the time periods scale as $m^{1/2}$. A secure detection of a planet probably requires at least half a dozen points which deviate from the standard curve. This, to detect Jupiter-mass planets, observations should be made every ~ 4 hr. Detection of Neptune-mass planets requires hourly observations. As discussed below, these observations can begin when the source comes within about twice the Einstein radius, θ_*, of the lensing star. If 10^7 stars are observed, roughly 16 will lie within $2\theta_*$ of a disk star at any given time. These 16 stars could be imaged once per hour with a 36 inch (91 cm) telescope.

While observations from one site would be useful, there are advantages to be gained by observing from several sites. First, since the planetary events last a day or less, those which peak during the daytime are likely to be missed. Thus, two widely separated telescopes would nearly double the number of detections. Second, the bulge lies near the ecliptic. Thus, in the months near December, it is visible for only a few hours per night from any one location. At least during these months, it

would be much better to have a global network of telescopes each fractionally committed to the project, rather than one or two telescopes that were totally committed. Third, in view of the fleeting nature of the events, it would seem prudent to build in some redundancy in case of bad weather at a particular site. Thus, the optimal scheme would employ, say, a dozen telescopes. Each of these would be committed to carry out two observations per night. During the near-December season, these would be near dawn or dusk and in other seasons, at more favorable times. In case of bad weather at one sight, the two neighboring sights might be able to pick up the slack.

As discussed in § 3, most of the probability for detection of a planet occurs when the source is within an Einstein radius of the lensing star. Can the lensing event be recognized in time to initiate observations during this crucial period? According to equation (2.6), the magnification $a \sim 1.06$ at two Einstein radii, and $A \sim 1.34$ at one Einstein radius. For a solar mass lens, the source will spend about 1 month on this part of the rising light curve. Assuming individual photometry errors of ~ 0.08 mag, it should be possible to recognize a likely lensing event during the first week of this month. For very small lensing stars, ~ 0.1 $M_\odot$, the approximately 10 day rising light curve should still be long enough to allow recognition of the event before the source enters the Einstein ring of the lensing star.

6. CONCLUSIONS

In this work we have analyzed the magnitude variation of a bulge star which is being microlensed by a planetary system in the Galactic disk. In about a fifth of the microlensing events, solar-like system planets positioned halfway to the Galactic center will provide a noticeable signature on the source light curve. This large fraction results primarily from a coincidence between the Einstein radius of the Sun and Jupiter's orbital radius. Such a coincidence may be duplicated in other planetary systems because the Einstein radius and the expected position of the largest planet may scale with stellar mass in roughly the same way.

The ratio of planetary to stellar mass can be determined directly from the observations. In addition, if the lensing star is a G dwarf or earlier, its spectrum can be taken. From the spectral type and luminosity, one may determine the mass and distance of the star and thereby infer the mass of the planet and its projected distance from the star.

The typical planetary signal lasts of order a day or less. A dedicated monitoring program is therefore necessary to pick up the signal. A candidate system should be observed at least several times per day and the observations should be made from two or more sites to ensure 24 hour coverage. This highly intensive monitoring of individual lensing stars must be triggered by a less intensive (i.e., ~ 1 observation per night from one sight) but much more extensive $\sim 10^7$ bulge stars) program designed to find lensing candidates. Such extensive microlensing searches are planned for the near future (Alcock et al. 1992; Paczyński et al. 1992) and may identify of order 10 or more microlenses per year. The fact that the relatively expensive "triggering programs" are now being undertaken for reasons unrelated to planets makes the present time appropriate to begin a microlensing search for planetary systems.

We thank J. Bahcall, B. Paczyński, N. Tyson, and J. Wambsganss for useful discussions. D. Stevenson suggested the scaling argument between Einstein radius and largest planet. This work was supported in part by a W. M. Keck foundation fellowship (A. L.) and an NSF contract PHY91-06210 (A. G.).

REFERENCES

Abramowitz, M., & Stegun, I. E. 1972, Handbook of Mathematical Functions, (Washington: National Bureau of Standards), 17
Alcock, C., et al. 1992, in preparation
Binney, J., & Tremaine, S. 1987, Galactic Dynamics (Princeton: Princeton Univ. Press), 17
Blandford, R. D., & Kochanek, C. S. 1987, Dark Matter in the Universe: Proc. Fourth Jerusalem Winter School for Theoretical Physics, ed. J. Bahcall, T. Piran, & S. Weinberg (Singapore: World Scientific), 139
Griest, K., et al. 1991, ApJ, 372, L79
Mao, S., & Paczyński, B. 1991, ApJ, 374, L37
Paczyński, B. 1991, ApJ, 371, L63
Paczyński, B., et al. 1992, in preparation
Scalo, J. M. 1986, Fund. Cosmic Phys., 11, 1
Stevenson, D. J. 1991, ARA&A, 29, 163
Stevenson, D. J., & Lunine, J. I. 1988, Icarus, 75, 146
Wolszczan, A., & Frail, D. A. 1992, Nature, 355, 145